Simulation of Multicomponent Evaporation in Electron Beam Melting and Refining*

A. Powell** J. Van Den Avyle B. Damkroger J. Szekely**

Liquid Metal Processing Laboratory, MS 1134, Sandia National Laboratories, PO Box 5800, Albuquerque, NM 87185. Phone: (505) 845-3105, Fax: (505) 845-3430.

**Massachusetts Institute of Technology, 77 Massachusetts Ave. Rm. 8-135, Cambridge. Massachusetts 02139. Phone: (617) 253-3222/3236, Fax: (617) 253-8124.

Abstract

Experimental results and a mathematical model are presented to describe differential evaporation rates in electron beam melting of titanium alloys containing aluminum and vanadium. Experiments characterized the evaporation rate of commercially pure titanium, and vapor composition over titanium with up to 6% Al and 4.5% V content as a function of beam power, scan frequency and background pressure. The model is made up of a steady-state heat and mass transport model of a melting hearth and a model of transient thermal and flow behavior near the surface. Activity coefficients for aluminum and vanadium in titanium are roughly estimated by fitting model parameters to experimental results. Based on the ability to vary evaporation rate by 10-15% using scan frequency alone, we discuss the possibility of on-line composition control by means of intelligent manipulation of the electron beam.

*This work performed at Sandia National Laboratories is supported by the U. S. Department of Energy under contract number DE-AC04-94AL85000.

Introduction

Although the electron beam cold hearth melting and refining process (shown schematically in figure 1) is extensively and increasingly used for the production of commercially pure (c.p.) titanium [1] [2], its use in producing titanium alloys has been limited by poor control of ingot composition which necessitates subsequent homogenization [3] [4]. This is due in part to irregularities in feed chemistry, which can be adjusted on-line, but also to frequent freezing and remelting of metal in the hearth and changes in throughput rate, which are very difficult to control.

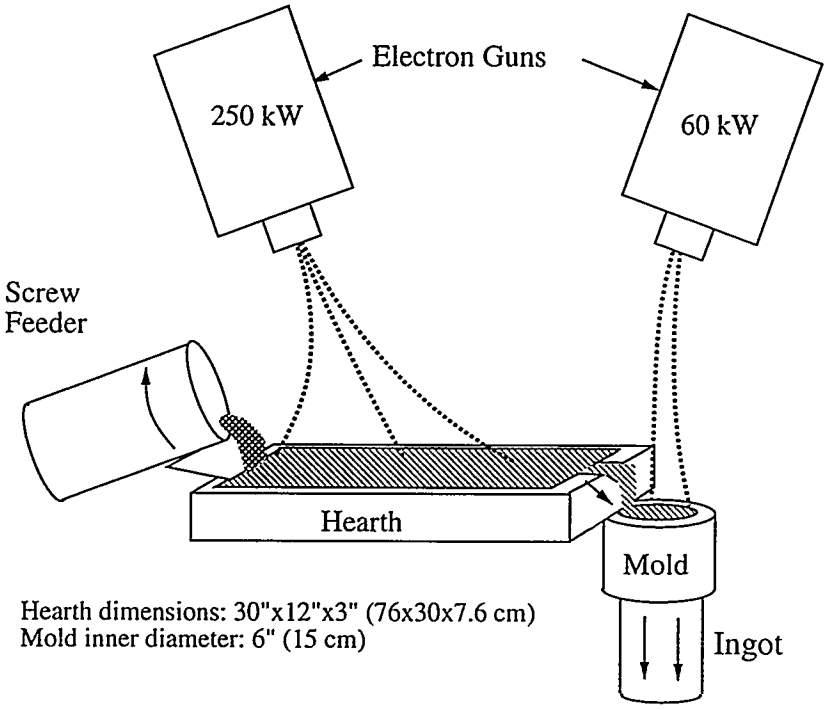

Figure 1: Electron beam melting facility at Sandia National Laboratories.

Because of this, control of composition downstream in the process could be very beneficial to electron beam melting of titanium alloys. The effect of beam scan frequency on evaporation rate, which has been extensively demonstrated experimentally [5] [6] [7]. may prove to be a means of establishing such downstream control. The development of a process model is thus in progress, both to evaluate potential use of scan frequency in composition control, and if it appears promising, to aid in the development of a suitable on-line control system.

The work described here includes experiments necessary for development of such a model, resulting in estimates for the activity of aluminum and vanadium in titanium and characterization of evaporation rate, and also a surface layer model for the estimation of enhanced evaporation rate due to transient heating by the scanning beam.

Experiments

Two sets of experiments were run in the hearth of the Sandia National Laboratories Liquid Metal Processing Laboratory electron beam furnace. These examined the effect of process parameters on evaporation rate of c.p. titanium, as measured by vapor condensation rate a known distance above the melt surface, and on the relationship between melt

and vapor chemistry in Ti-Al-V melting. The 250 kW gun was used alone at power levels from 150 to 265 kW, scan frequencies from 30 to 450 Hz, and beam spot size set from approximately 2 to 4 cm (though attempts to measure the actual spot size were unsuccessful), under background argon pressure between 0.13 and 40 Pa (10^{-5} to 3×10^{-3} torr).

Measurements of c.p. titanium evaporation rate were begun by holding process parameters constant for at least seven minutes in order to achieve steady-state pool geometry and skull heat transfer conditions. A water-cooled probe with vapor condensation substrate was then inserted to a known position and orientation in the furnace for approximately sixty seconds, and subsequently withdrawn. Thicknesses of films thus deposited were measured by optical microscopy of sectioned substrates.

In the alloy experiments, composition variation was achieved by starting the beam over a charge of as-received Ti-6%Al-4%V and taking melt and vapor condensate samples periodically as aluminum evaporated preferentially out of the melt, moving the composition down along the gray line shown in figure 2. After this, a steady state composition was established by melting alloy scrap and flowing it through the hearth to build an ingot at a constant rate, so that vapor samples at various beam and chamber conditions could be taken with constant melt composition. Finally, c.p. titanium was slowly added to the hearth in order to obtain melt and vapor samples at low vanadium concentrations. Electron probe microanalysis was used to determine the composition of all samples.

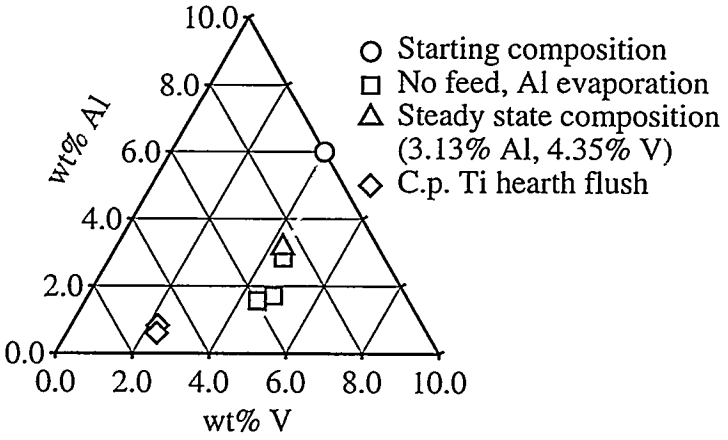

Figure 2: Hearth melt compositions for alloy experiments, shown in the Ti-Al-V system.

Experimental Results

Figure 3 shows the variation of pure titanium condensation rate at the substrate with process parameters. Inspection of the graph reveals the expected rise in evaporation rate with increasing beam power and decreasing spot size. Chamber pressure presents competing effects of gas focusing of the beam and interference with evaporant transport. However, the frequency correlation is the opposite of what was expected. Further analysis of the process showed that our beam deflection system could not track the imposed pattern at the highest frequencies, so the resulting pattern was narrower and considerably more intense, leading to an increase in maximum temperature and evaporation rate.

In order to separate out the effect of pattern size on evaporation rate, we calculated an expected evaporation rate by integrating Langmuir evaporation rates over temperature maps of the hearth surface taken at 30 and 450 Hz [8]. Based on this method, the temperature profile arising from the 450 Hz pattern is expected to lead to a 44% higher evaporation

rate than at 30 Hz. The average observed rise of 25% at 0.13 Pa thus shows a net decrease of approximately 19% due to increased scan frequency.

Melt and vapor compositions were measured as described above, and are summarized in figure 4. The "evaporation ratio" ER shown in figure 4 is defined (for aluminum) as

$$ER_{\mathrm{Al}} = \frac{\mathrm{wt\%Al_{vapor}/wt\%Ti_{vapor}}}{\mathrm{wt\%Al_{melt}/wt\%Ti_{melt}}}. \tag{1}$$

This is used because it can be shown [9] that this evaporation ratio is equivalent to

$$ER_{\mathrm{Al}} = \gamma_{\mathrm{Al}} \frac{\bar{p}_{v\mathrm{Al}}}{\bar{p}_{v\mathrm{Ti}}} \sqrt{\frac{M_{\mathrm{Ti}}}{M_{\mathrm{Al}}}}, \tag{2}$$

where γ_i is the activity coefficient, $\bar{p}_{vi}$ is the vapor pressure of pure species i, and M_i its molecular weight, as long as aluminum activity follws Henry's law. Because these material properties do not vary with composition, the evaporation ratio is not expected to do so.

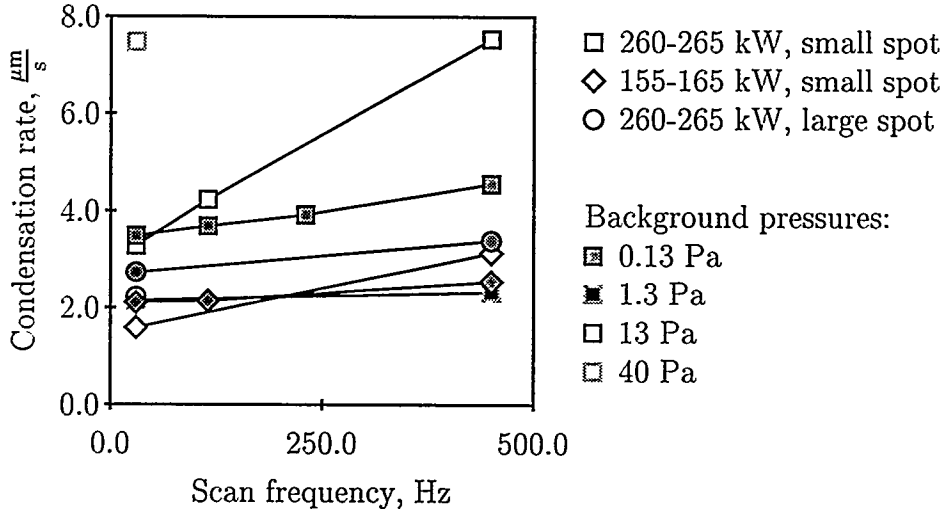

Figure 3: Effect of process parameters on measured condensation rate of pure titanium.

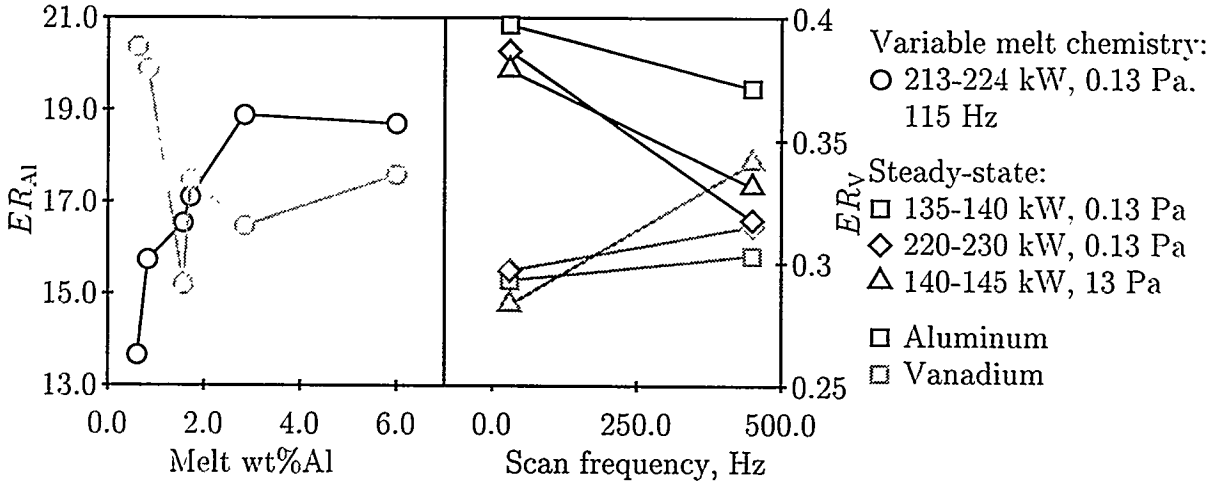

Figure 4: Effect of melt composition and process parameters on measured evaporation ratios of aluminum and vanadium in titanium.

Measured evaporation ratios fell in the range of 16-21 for aluminum and 0.28 to 0.34 for vanadium over the range of process parameters used in the steady-state experiment. The ratio of pure element vapor pressures varies considerably, from just over 800 at the melting point of titanium to around 140 at a 500°C superheat for aluminum, and from 0.16 to 0.37

over the same temperature range for solid vanadium (vapor pressure of undercooled liquid vanadium at these temperatures is not available).

Aluminum evaporation ratios were found to decrease with increasing scan frequency, increasing beam power, increasing background gas pressure, and decreasing Al and V content; Vanadium exhibited the opposite tendencies, presumably because of its lower evaporation rate than that of titanium. From these correlations, it would seem that the aluminum evaporation ratio is falling with increasing surface temperature, so the decreasing pure vapor pressure ratio controls that change. It is interesting that although the evaporation ratio is related to chemical parameters that are independent of composition, the biggest change in both evaporation ratios occurred when the vanadium concentration changed (figure 4: figure 2 indicates the lowest Al concentration coincides with very low V).

In order to calculate the activity coefficient γ_{Al}, we consider the quantity $\frac{\bar{p}_{v\mathrm{Al}}}{\bar{p}_{v\mathrm{Ti}}}\sqrt{\frac{M_{\mathrm{Ti}}}{M_{\mathrm{Al}}}}$, which is equal to $ER_{\mathrm{Al}}/\gamma_{\mathrm{Al}}$ and is a function of temperature alone. The average value of that quantity over a hearth surface temperature map is 317 at 30 Hz and 283 at 450 Hz. Based on average aluminum evaporation ratios of 20.3 at 30 Hz and 17.8 at 450 Hz, this gives us activity coefficients of 0.0640 and 0.0628 respectively. The same treatment for vanadium gives average ratios of 0.312 and 0.293, and dividing the average ER_{V} values of 0.291 and 0.320 by these yields activity coefficients for solid vanadium of 0.993 and 1.027. which indicates approximately ideal behavior of V in molten Ti.

Surface Layer Heat Transfer and Evaporation

When considering the beam's ability to control composition, one must consider both composition limits which the beam can produce under steady-state conditions, and the dynamic ability to vary composition between those limits in response to process changes. Dynamic control will be covered in a later paper, so we turn here to the steady-state case.

In a continuous solute removal reactor such as a melting hearth, the ratio of solute concentration at the exit to that at the inlet $C_{\mathrm{out}}/C_{\mathrm{in}}$ is a function of flow rate Q, reaction area A, and the reaction rate constant k'' (equal to the solute flux divided by concentration). The nature of this function will depend on the flow patterns present in the hearth, with the extremes in behavior being a perfect mixing tank, which behaves as

$$\frac{C_{\mathrm{out}}}{C_{\mathrm{in}}} = \frac{1}{1+\frac{k''A}{Q}}, \tag{3}$$

and a plug flow reactor, which gives

$$\frac{C_{\mathrm{out}}}{C_{\mathrm{in}}} = \exp\left(-\frac{k''A}{Q}\right). \tag{4}$$

If we neglect dead zones in the flow pattern, the relevant area is the molten area of the hearth, and flow rate is given by throughput divided by density. The reaction rate constant for species i in solvent s is calculated as the ratio of Langmuir evaporation rate to molar density in the melt, and since Henrian vapor pressure is given by $\gamma_i \bar{p}_{vi} X_i$ (using the same definitions as equations 1–2), this gives

$$k_i'' = \frac{\text{molar flux}}{\text{molar density}} = \frac{\frac{\gamma_i \bar{p}_{vi} X_i}{\sqrt{2\pi M_i RT}}}{X_i \frac{\rho_s}{M_s}} = \frac{M_s}{\rho_s}\frac{\gamma_i \bar{p}_{vi}}{\sqrt{2\pi M_i RT}}. \tag{5}$$

For aluminum in titanium, the reaction rate constant k''_{Al} takes on values from 6.19 $\frac{\mu\mathrm{m}}{\mathrm{s}}$ at the melting point of titanium to 239 $\frac{\mu\mathrm{m}}{\mathrm{s}}$ at a 500°C superheat. Using top surface

temperature maps of the hearth at Sandia [8], we calculate an average k''_{Al} of $98.3\frac{\mu m}{s}$ at 30 Hz, and combining this with a typical flow rate of 23 $\frac{cm^3}{s}$ and top surface area of 0.2 m^2 gives the ratio $\frac{k''A}{Q}$ as 0.86. This will lead to retention of 42% of the aluminum under plug flow conditions, and 54% under perfect mixing, the latter of which agrees well with 52% retention (3.13% ÷ 6%) observed in the steady state alloy chemistry experiment.

We now consider the effect of beam frequency on the time-averaged reaction rate constant. When the transient motion of the beam has an effect on the evaporation characteristics, modeling such characteristics would seem at first to require a time-stepped simulation of the beam's travels over the whole hearth, which would be extremely computationally intensive. However, if the beam moves through the pattern relatively quickly, the depth of the layer heated during one complete scan will be much smaller than the width of the beam spot, and as long as the Peclet number is small (indicating transient thermal convection can be neglected), vertical conduction will dominate heat transfer away from the surface.

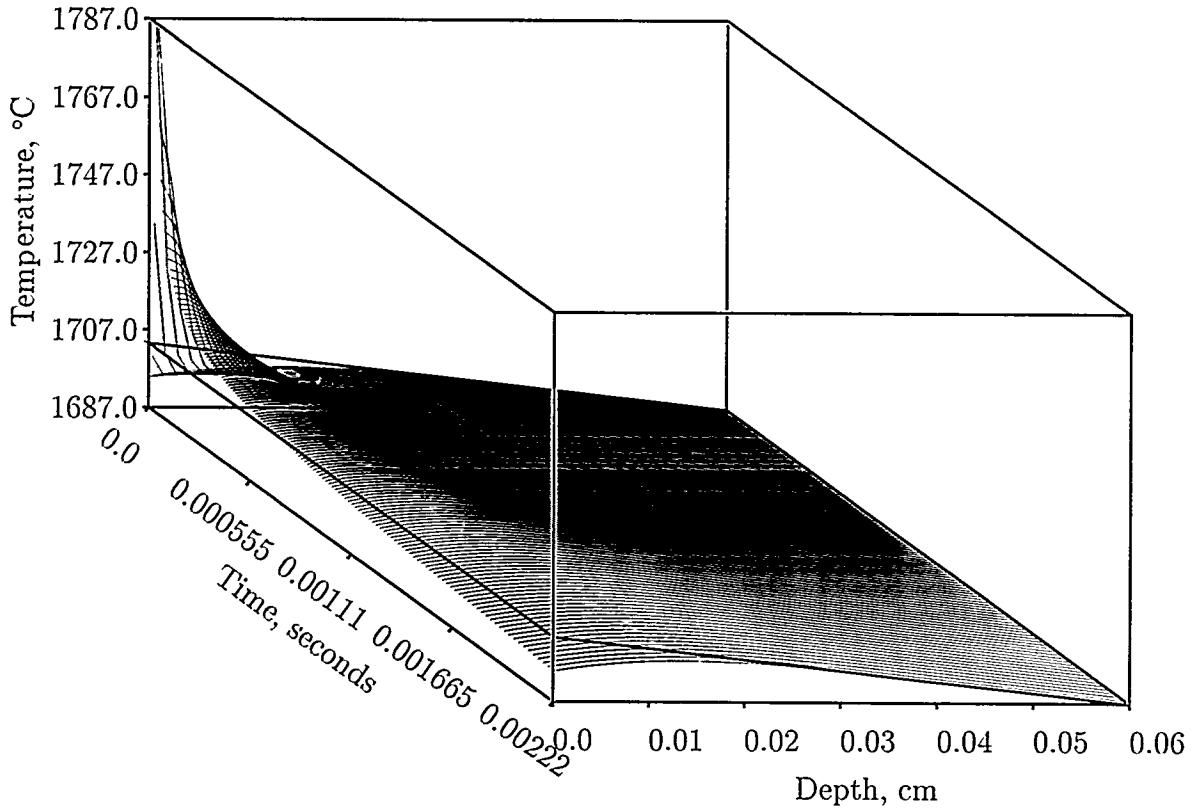

Figure 5: Calculated temperature history in the top surface layer of molten titanium hit by a 150 kW (net) beam at 450 Hz. For clarity, only every other timestep is shown here.

For this reason, temperature fluctuations near the surface can be considered locally one-dimensional, and the increase in losses for a given average surface temperature can be calculated by simply solving the heat conduction equation in one dimension. Unfortunately, the highly nonlinear nature of thermal losses at the surface makes the problem analytically intractable, but it is an easy problem to solve numerically, as has been done here.

The program written to solve this problem simulates transient heat transfer through the top layer of the melt, down to a depth $\delta_T = 4\sqrt{\alpha t}$ where α is the thermal diffusivity and t is the period of beam rastering (the inverse of the frequency). Below this depth, temperature does not change significantly. On the bottom of this surface layer temperature is held constant. On the top, heat flux is given by the difference between heat input from the

beam and losses due to radiation and evaporation. The beam is modeled as the projection of a traveling Gaussian heat flux onto a point, which is thus a Gaussian distribution in time. Evaporation rate is assumed to follow ideal Langmuir evaporation into a vacuum.

This top surface layer simulation runs through several beam scan cycles until convergence is reached. A typical history for the last cycle of such a simulation is shown in figure 5. For accurate coupling with thermofluid simulations of the molten hearth, which linearize temperature distribution near the surface, a tangent line in the temperature-depth curve is drawn at the bottom of the simulated layer, and its intercept with the surface is considered to be the average surface temperature, as can be seen on figure 5. The time-averaged evaporative flux for a given species in solution is calculated from the surface temperature history, and plotted against the average surface temperature for several frequencies, as shown in figure 6.

For the simulations presented here, net beam power (less backscattering losses) was set to 150 kW, spot diameter to 2 cm, and overall scan pattern length to 2 m. Under these conditions, peak power density is about 24 kW/cm^2, and dwell time is one hundredth the beam scan period. Figure 6 shows calculated pure titanium evaporation rate ($\frac{\text{kg}}{\text{m}^2\cdot\text{sec}}$) and aluminum reaction rate coefficient at three different frequencies and using the latter definition of average surface temperature. It is worth noting that evaporation rates at 450 Hz are not significantly different from those at constant temperature for titanium.

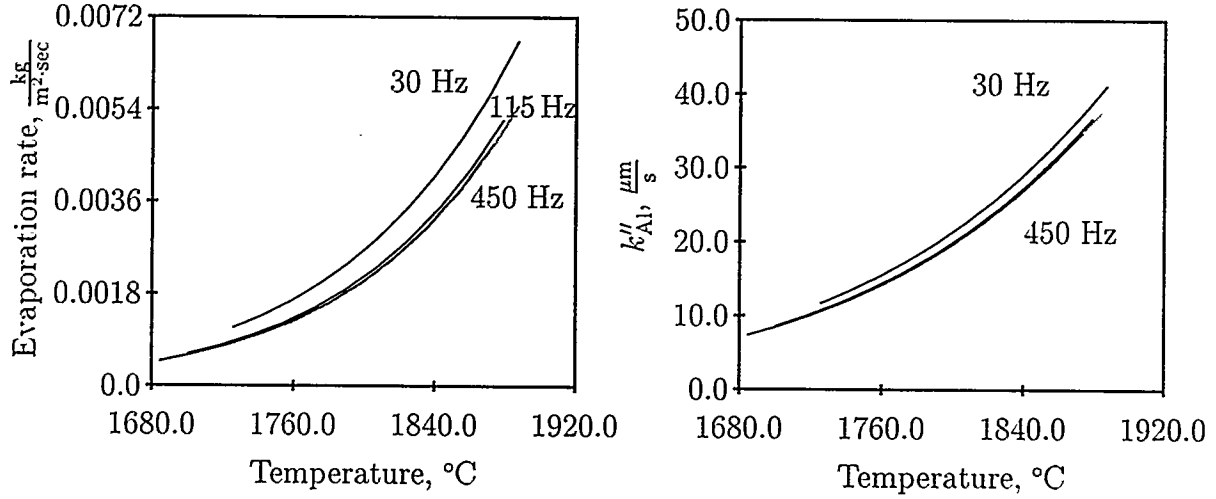

Figure 6: Calculated pure titanium evaporation rates and aluminum reaction coefficients due to a 150 kW (net) beam as a function of average surface temperature at 30, 115 and 450 Hz. The gray curves represent constant temperature evaporation rate.

Also, calculated increases in titanium evaporation at 30 Hz above constant temperature, which are about 40% near the melting point and 25% at a 200°C superheat, are of the same order of magnitude as the 19% net increase calculated from experimental data, and a 17% increase in titanium evaporation rate measured by Melde *et al.* [7, p. 79], when going from 20 ms to 300 ms dwell time. The higher values predicted by the model are due to the fact that the model deals with losses directly in the path of the beam, while most of the hearth is not in that path and will not exhibit such strong temperature fluctuations.

This frequency change has a somewhat smaller effect on the time-averaged aluminum reaction rate constant k''_{Al}, which is at most 11% higher at 30 Hz than at 450 Hz. Because aluminum concentration change varies with k''_{Al}, they will scale similarly; in the case of the Sandia furnace we can expect to be able to vary the concentration 5% (perfect mixing) to 10% (plug flow) by changing beam scan frequency alone.

Conclusions

Activity coefficients of aluminum and vanadium in titanium have been estimated at 0.063 and 1.0 based on melt and condensed vapor compositions and hearth temperature profiles. The only assumptions required for this estimation are Henrian behavior of the solutes and equal distribution of all three constituent elements throughout the vapor plume.

In addition, the mathematical model presented here gives a good estimate of the effect of beam scan frequency on pure titanium evaporation rate and aluminum activity. Based on this model, we conclude that because aluminum reactivity is not very sensitive to scan frequency, scan frequency alone probably can not produce the desired changes in composition, and it will be necessary to explore alternative pattern designs which produce large changes in evaporation rate without significantly affecting fluid flows and skull shape. The design of such patterns will require the coupling of this surface model with a more comprehensive model of fluid flow and heat transfer in the hearth or mold.

It is important to note that implementation of the type of process control described here will require the use of a beam deflection system capable of tracking patterns at very high frequencies, which is possible but somewhat expensive; and on-line measurement of melt chemistry, which is extremely difficult. These two considerations may hinder practical use of this technique for the foreseeable future.

References

[1] S.M. Tilmont and H. Harker, "Maximelt, an Update" (Paper presented at Electron Beam Melting and Refining State of the Art 1993), 214-225.

[2] DS. Lowe, "Electron Beam Cold Hearth Refining in Vallejo" (Paper presented at Electron Beam Melting and Refining State of the Art 1994), 69-77.

[3] J.C. Borofka, "Qualification of the 3.3 MW Maximelt EBCHR Furnace for Premium Quality Titanium Alloys" (Paper presented at Electron Beam Melting and Refining State of the Art 1992), 179-189.

[4] Dr. Entrekin, Axel Johnson Metals, private communication with author, TMS Annual Meeting, 14 February 1995.

[5] S. Schiller, A. von Ardenne and H. Förster. "Evaporation of Alloying Elements in EB-Melting–Possibility of Influence" (Paper presented at Electron Beam Melting and Refining State of the Art 1984), 49-69.

[6] M. Blum *et al.*, "Results of Electron Beam Remelting of Superalloys and Titanium Alloys with a High-Frequency EB-Gun" (Paper presented at Electron Beam Melting and Refining State of the Art 1993), 102-115.

[7] C. Melde, M. Kramer, A. von Ardenne and M. Neumann, "The Super Deflection System – a Tool to Reduce the Evaporation Losses in EB Melting Process" (Paper presented at Electron Beam Melting and Refining State of the Art 1993), 69-80.

[8] M. Miszkiel, R. Davis, J. Van Den Avyle and A. Powell "Video Imaging and Thermal Mapping of the Molten Hearth in an Electron Beam Melting Furnace" (Paper presented at Electron Beam Melting and Refining State of the Art 1995).

[9] A. Powell *et al.*, "Simulation of Multicomponent Losses in Electron Beam Melting and Refining at Varying Scan Frequencies" (Paper presented at Electron Beam Melting and Refining State of the Art 1995).

DISCLAIMER